Title of article:

Effect of Ag-doping on crystal structure and high temperature thermoelectric properties of *c*-axis oriented $Ca_3Co_4O_9$ thin films by pulsed laser deposition

Authors and address:

T. Sun[1], H. H. Hng[1,*] , Q. Y. Yan[1] and J. Ma[1,2]

[1]School of Materials Science and Engineering, Nanyang Technological University, Singapore 639798

[2]Temasek Laboratories, Nanyang Technological University, Singapore 637553

Abstract

Ag-doped $Ca_3Co_4O_9$ thin films with nominal composition of $Ca_{3-x}Ag_xCo_4O_9$ (x = 0~0.4) have been prepared on sapphire (0001) substrates by pulsed laser deposition (PLD). Structural characterizations and surface chemical states analysis have shown that Ag substitution for Ca in the thin films can be achieved with doping amount of $x \leq 0.15$; while when $x > 0.15$, excessive Ag was found as isolated and metallic species, resulting in composite structure. Based on the perfect *c*-axis orientation of the thin films, Ag-doping has been found to facilitate a remarkable decrease in the in-plane electrical resistivity. However, if doped beyond the substitution limit, excessive Ag was observed to severely reduce the Seebeck coefficient. Through carrier concentration adjustment by Ag-substitution, power factor of the Ag-$Ca_3Co_4O_9$ thin films could reach 0.73 $mWm^{-1}K^{-2}$ at around 700 K, which was about 16% higher than that of the pure $Ca_3Co_4O_9$ thin film.

Key words:

Thermoelectric; Ca3Co4O9; Thin film; Doping

* Corresponding author. Tel.: +65 6790 6214; fax: +65 6790 9081

E-mail address: asjma@ntu.edu.sg (J. Ma)

1. Introduction

Thermoelectric (TE) materials and devices have great potential to provide alternative solutions to worldwide energy crisis and global warming, as they are able to harvest clean energy from waste heat and provide refrigeration without using harmful gas. Among the various TE materials, misfit layered cobalt oxide $Ca_3Co_4O_9$ has been considered to be the most promising candidates for high temperature TE application due to its remarkable TE performance and superior properties, such as low toxicity, high thermal stability and low cost [1]. The performance of a TE material is evaluated by the dimensionless figure-of-merit $ZT = S^2T/(\rho\kappa)$, where S, T, ρ and κ are the Seebeck coefficient (also called thermopower), absolute temperature, electrical resistivity and thermal conductivity, respectively [2]. For a $Ca_3Co_4O_9$ single crystal, the ZT value can reach 0.83 at 1000 K [3].

The crystal structure of $Ca_3Co_4O_9$ is composed of the CdI_2-type CoO_2 layer and the rock-salt-type Ca_2CoO_3 layer alternately stacking along the *c*-axis [4]. Although this misfit layered structure is considered to be beneficial for TE properties, the large anisotropy leads to poor TE performance for randomly oriented polycrystalline materials, and difficulty in fabricating large $Ca_3Co_4O_9$ single crystals for volume production [5]. Nevertheless, it is found that thin film configuration with well controlled crystal orientation can cater for the electrical transport of carriers along favorable direction and overcome this issue. In addition, thin films can promote the reduction of thermal conductivity by phonon scattering effect [6], and facilitates Micro-Electro-Mechanical System (MEMS) processing towards on-chip devices [7]. Epitaxial or *c*-axis oriented $Ca_3Co_4O_9$ thin films have been prepared by various techniques, such as radiofrequency (RF) sputtering [8], pulsed laser deposition (PLD) [9, 10], atomic layer deposition (ALD) [11] and topotactic ion-exchange method [12]. The in-plane power factor of a pure $Ca_3Co_4O_9$ thin film has been reported to reach 0.51 $mWm^{-1}K^{-2}$ at around 920 K, which is higher than the value of textured bulk ceramics, and comparable to that of single crystals [13]. Such improvement in TE performance could be ascribed to the enhanced energy filtering effect as a result of the nanostructures and grain boundaries inside the thin films [9, 13].

Meanwhile, research work towards TE performance enhancement in $Ca_3Co_4O_9$ bulk

materials have also been carried out through foreign cation-doping using alkali metals [14], alkaline earth metals [15], rare earths [16, 17] and transition metals [18]. Among them, Ag-substitution at the Ca site has been found to effectively reduce the electrical resistivity of $Ca_3Co_4O_9$, and thus improve the TE performance [19]. It has also been found that if Ag is not doped into the $Ca_3Co_4O_9$ lattice, but instead is added as a metallic phase to form bulk composite ceramics, a decrease in electrical resistivity can still be achieved [20, 21]. Through the doping and the addition of Ag, a high *ZT* value above 0.5 at 1000 K has been reported in $Ca_{2.7}Ag_{0.3}Co_4O_9$/Ag-10%, which is so far the highest *ZT* value reported for polycrystalline $Ca_3Co_4O_9$ system [22]. It should be noted that although both approaches can reduce electrical resistivity, different mechanisms are involved: Ag-substitution increases p-type major carrier concentration; while metallic Ag addition contributes to electrical conduction by composite effect. It is therefore necessary to identify the exact amount of Ag substituted and to fully characterize the Ag dopant species in heavily Ag-doped $Ca_3Co_4O_9$ system. As indicated in previous works, having a thin film configuration of such material can facilitate the above mentioned characterization using XPS and Hall effect analysis [23]. In this work, we report the Ag-doping effect and TE enhancement in *c*-axis oriented $Ca_3Co_4O_9$ thin films. The Ag-doping level and dopant species are fully characterized. The influences of light and heavy Ag-doping on carrier concentration as well as high temperature electrical properties of these thin films are also investigated.

2. Experimental details

$Ca_{3-x}Ag_xCo_4O_9$ (x = 0, 0.1, 0.2, 0.3 and 0.4, named as CCO, Ag01, Ag02, Ag03 and Ag04 respectively in the subsequent text) thin films with *c*-axis orientation were prepared on (0001) sapphire (*c*-plane) single crystal substrates by PLD method at 700°C in 20 Pa (150 mTorr) oxygen pressure. A KrF excimer laser (Lambda Physik Compex, λ = 248 nm) was used with a laser energy density of ~1.2 J/cm^2 per pulse corresponding to a deposition rate around 2 nm/min. To prepare the PLD targets, the $Ca_{3-x}Ag_xCo_4O_9$ precursor powders were first synthesized by sol-gel method [17], then shaped into 1-inch diameter pellets and sintered at 880°C for 20 hours. Due to the strong volatile nature of Ag during PLD process [24], double

amounts of the designed composition of Ag were added in the targets. Chemical compositions of the targets, obtained by inductively coupled plasma (ICP) analysis (Dual-view Optima 5300 DV ICP-OES, Perkin Elmer), are listed in Table 1 with the corresponding sample names and the elemental ratio in the precursor solutions.

The thicknesses of the thin films were measured using an Alpha-Step IQ surface profiler. High resolution X-ray diffraction (HR-XRD) data were collected using X'Pert MRD (PANalytical) with monochromatic Cu $K\alpha$ radiation (λ = 1.5406Å) over 5~55° range. Chemical states and elemental composition were analyzed by using an X-ray photoelectron spectroscopy (XPS) (Al anode, hv = 1,486.6 eV, Theta Probe XPS, Thermo Fisher Scientific) on the thin film surfaces. The C 1s peak located at 284.5 eV was assigned to carbon from adventitious contaminations, and was used as the criterion to rectify binding energies of the XPS spectra. The in-plane electrical resistivity (ρ_{ab}) and Seebeck coefficient (S) of the thin films were measured from room temperature to ~700 K by the standard four-probe method and the conventional steady state method, respectively. Room temperature carrier concentrations (p) of the thin films were determined by the Hall measurement (Bio Rad HL5500) with four-point-probe technique using van der Pauw geometry.

3. Results and discussion

Fig. 1 shows the HR-XRD 2θ–ω scans of pure and Ag-doped $Ca_3Co_4O_9$ thin films on (0001) sapphire substrate over 5~55° range. Thin films Ag01 and Ag02 show similar XRD patterns to that of the pure thin film, CCO. Besides the peak from sapphire (0006) substrate, only peaks from diffractions of (00l) $Ca_3Co_4O_9$ planes can be observed, indicating that the *ab*-planes in the $Ca_3Co_4O_9$ thin films are parallel to the (0001) sapphire substrate surface and both films are *c*-axis oriented. However, for thin films Ag03 and Ag04, an extra peak at ~38.12° can be observed. This peak corresponds to Ag (111), which indicates the presence of Ag existing as a metallic phase other than those doped into the $Ca_3Co_4O_9$ crystal structure. The influence of Ag-doping on the crystal lattice of $Ca_3Co_4O_9$ thin films was investigated by calculating the *c*-axis parameters of the pure and Ag-doped $Ca_3Co_4O_9$ thin films from the

XRD data. For each thin film, the average *c*-axis parameter was calculated by using Bragg equation according to every position of the (00*l*) peaks in the HR-XRD pattern. It can be seen from Fig. 2 that the *c*-axis lattice constant increases gradually with the Ag amount (as determined by XPS). The ionic radii of Ag^{1+} and Ca^{2+} in six-coordination are 1.15 and 1.00 Å, respectively [19]. Thus, for light Ag-doping, the substitution of the larger Ag^{+} ions for Ca^{2+} can result in the enlargement of the $Ca_3Co_4O_9$ unit cell. This observation is consistent with the reported work on Ag-substituted $Ca_3Co_4O_9$ poly-crystals [19]. However, it is found that the *c*-lattice parameter of $Ca_3Co_4O_9$ thin films continues to increase for the heavily Ag-doped samples beyond the Ag-substitution limit (as indicated in the subsequent XPS analysis). Such *c*-direction expansion is likely to be associated with the thin film strain relaxation [25, 26]. Due to the lattice misfit from substrate, the *c*-axis lattice parameter of the highly oriented $Ca_3Co_4O_9$ thin films (10.73~10.79 Å in this work, and 10.73~10.78 Å in others [10-12]) is slightly lower than that of the bulk value (10.81~10.99 Å [4, 15, 19]). In the case of heavy Ag-doping, Ag segregation or crystallization can introduce large amount of structural defects and can release the thin film strain from the substrate. Thus, as the Ag-dopant further increases, the *c*-lattice of thin film starts to be relaxed and increases towards the value of the bulk.

In order to study the doping effect on TE properties, the exact amounts of Ag dopant in these thin films were determined by using the area ratios of Ca ($2p_{3/2}$), Co ($2p_{3/2}$), and Ag ($3d_{5/2}$) peaks. The results are summarized in Table 1. It is found that, even after doubling the amount of Ag in the targets, the final Ag compositions in the resultant as-prepared thin films were still lower than the designed values, indicating that a substantial amount of Ag atoms were "lost" during the PLD process. The yield of Ag by the laser ablation is only about 36% in this thin film fabrication process (with reference to the yield of Co taken as 100%). Further, the chemical states of Ag dopant within the Ag-$Ca_3Co_4O_9$ thin films were investigated by XPS fine scan of the Ag 3d peaks, as shown in Fig. 3. For thin films Ag01 and Ag02, the peaks of Ag $3d_{3/2}$ and $3d_{5/2}$ are located at 373.7 and 367.7 eV, respectively, and the spin energy separation is 6.0 eV. This is the characteristic of Ag–O bond [27], indicating that the silver

species existing in these two thin films is Ag^{+} ion rather than metallic Ag (Ag^{0}). It should be noted that Ag oxide will decompose into metallic Ag at temperatures above 400°C, while the deposition of the Ag-doped $Ca_3Co_4O_9$ thin films was carried out on a substrate at 700°C. Thus, neither Ag_2O nor AgO phases would be generated in the PLD process and all the Ag^{+} ions in samples Ag01 and Ag02 should come from the Ag^{+} substituted at Ca site in the $Ca_3Co_4O_9$ crystal structure. In other words, it can be concluded that most Ag atoms in thin films Ag01 and Ag02 have successfully substituted into the Ca site in the crystal structure. On the other hand, for samples Ag03 and Ag04, the 3d peaks of Ag in the XPS spectra are found to shift to higher binding energy, indicating that chemical states of Ag atoms are not uniform in these two $Ca_3Co_4O_9$ thin films. The Ag 3d peaks were further decomposed into two components, Ag^{+} with binding energy of 373.7 and 367.7 eV, and Ag^{0} with binding energy of 374.2 and 368.2 eV [27], as shown in Fig. 3. The Ag^{+} : Ag^{0} atomic ratio were calculated based on the $3d_{5/2}$ peaks deconvolution using Gaussian–Lorentzian sum functions and Tougaard-type background subtraction, and the results are listed in Table 1. It can be found that with heavy doping of Ag, some metallic Ag^{0} atoms are present in the Ag03 and Ag04 films. Moreover, as the Ag content in the thin films increases, the amount of Ag^{0} is found to increase significantly, while there is only a slight increase for the substitution amount, Ag^{+}. These XPS results clearly indicated that the Ag contents for thin films Ag03 and Ag04 have gone beyond the substitution limit of Ag in the $Ca_3Co_4O_9$ crystal structure. The excess amount of Ag atoms exists as metallic Ag^{0} phase within the thin films, which is consistent with the XRD results.

A recent work done on Ag-doped $Ca_3Co_4O_9$ poly-crystalline bulk samples prepared by conventional solid state reaction route reported heavy Ag-doping of nominally 10 at% at the Ca site (corresponding to x = 0.3 in $Ca_{3-x}Ag_xCo_4O_9$) [19]. However, the exact amount of Ag in $Ca_3Co_4O_9$ was not provided and the characterization on the species of the Ag-dopant was limited. According to our study, a lower Ag-substitution limit in the $Ca_3Co_4O_9$ structure was suggested to be about 5 at%. First of all, it should be noted that the radius of Ag^{+} ion (1.15 Å) is much larger than that of Ca^{2+} (1.00 Å) ion. The substitution of Ag for Ca, or any possible interstitial Ag atom, can lead to large lattice distortion accompanied with a large increase in

the system energy. Thus, heavy-doping of Ag is not favorable in the $Ca_3Co_4O_9$ structure. Furthermore, due to the weak Ag–O bond at high temperature, Ag cannot combine with oxygen. So, it will be difficult for Ag atoms to get into the $Ca_3Co_4O_9$ structure through high-temperature processing routes. It is hence unlikely to achieve heavy Ag^+ substitution through either solid state reaction or PLD methods. In addition, in the case of PLD fabrication, the dissociative Ag atoms are unstable at high temperature under vacuum and tend to evaporate from the substrate surface. As a result, the deposition yield of Ag is fairly low and the as-prepared thin films possess less Ag content than in the corresponding targets.

The temperature dependence of the in-plane electrical resistivity, ρ, of the pure and Ag-doped $Ca_3Co_4O_9$ thin films on sapphire (0001) was measured for the temperature range of 300 to 720 K. As shown in Fig. 4, all the thin film samples show a low electrical resistivity around 3.5~5.5 mΩcm over the temperature range measured. The ρ values of the thin films obtained in the present work are lower than that of the reported poly-crystalline $Ca_3Co_4O_9$ bulk (6~12 mΩcm) [22], and are comparable to that reported for single crystal [3]. The superior electrical conduction property is attributed to the highly oriented thin film structure achieved by PLD processing as previously reported [9, 23]. For thin films Ag01 and Ag02, electrical resistivity shows similar transport behavior to that of un-doped $Ca_3Co_4O_9$ thin film CCO, namely, metallic-like behavior at room temperature, and semiconducting-like behavior at elevated temperatures. Moreover, when compared with the pure $Ca_3Co_4O_9$ thin film, the resistivity of samples Ag01 and Ag02 decreases significantly with increasing Ag content within the entire temperature range measured, indicating that Ag substitution for Ca have efficiently reduced the ρ of the *c*-axis oriented $Ca_3Co_4O_9$ thin films. It is worth noting that the electrical resistivity of the Ag-doped $Ca_3Co_4O_9$ thin films obtained in this work is 3.86 mΩcm at ~675 K for Ag02, which is one of the lowest values reported thus far for $Ca_3Co_4O_9$ based materials. The electrical resistivity can be expressed as $\rho = 1/\sigma = 1/(\mu pe)$, where σ, p, μ and e are the electrical conductivity, p-type carrier concentration, carrier mobility and electron charge of carrier, respectively. As shown in the inset of Fig. 4, the increases in both p and μ by Ag-

substitution for Ca contribute to the superior electrical conduction property, which is consistent with that reported for Ag-doped $Ca_3Co_4O_9$ poly-crystalline bulk materials [22].

On the other hand, for thin films Ag03 and Ag04, the ρ–T curves exhibit metallic-like behavior in the entire measured temperature range. Although the electrical resistivity decreases with increasing Ag content at the low temperature range (300~550 K), the ρ values of samples Ag03 and Ag04 are higher than that of Ag02 at the high temperature range above 600 K. This is similar to that reported for $Ca_3Co_4O_9$ poly crystalline materials with Ag added as metallic phase [21, 22]. Further investigation through Hall effect measurement has indicated that the effective carrier concentration, p, for thin films Ag03 and Ag04 decreases with increasing Ag content. Thus, it can be concluded that further increase in Ag doping content results in composite effect since metallic Ag offers electron conduction in a p-type $Ca_3Co_4O_9$ semiconductor matrix.

Further study on the electrical conduction mechanism in these Ag-$Ca_3Co_4O_9$ thin films was carried out by data analysis using both thermally activated conduction (TAC) model and adiabatic small polaron hopping conduction (SPHC) model in the high temperature region for T > 550 K. As shown in Fig. 5, the plots of ln(ρ/T) versus 1000/T for all the samples lie on straight lines for temperatures above 550 K, indicating the SPHC behavior in these thin films. According to the SPHC mechanism of $Ca_3Co_4O_9$, the temperature dependence of electrical resistivity can be generally expressed as [18, 23]

$$\frac{1}{\rho} = \sigma = pea^2\left(\frac{A}{T}\right)\exp\left(\frac{-E_a}{k_B T}\right) \qquad \text{(Eq. 1)}$$

where a, E_a, k_B and A are the intersite distance of hopping, activation energy, Boltzmann constant and a pre-exponential term related to the scattering mechanism, respectively. From the slopes of the plots in Fig. 5, E_a of the pure and Ag-doped $Ca_3Co_4O_9$ thin films can be calculated, and the results are shown in the inset of Fig. 5. It can be seen that, for CCO, Ag01 and Ag02 films, E_a remains almost constant within the range of 71~73 meV, while E_a values of Ag03 and Ag04 samples are much lower, indicating the different conduction mechanism in

these two films. For the lightly Ag-doped thin films Ag01 and Ag02, the decrease of electrical resistivity can be attributed to the substitution of univalent Ag^{+} for divalent Ca^{2+} in $Ca_3Co_4O_9$. It has been reported that the edge shared CoO_2 layers are responsible for the electrical conduction, whereas the rock-salt-type [Ca_2CoO_3] layers are regarded as a charge reservoir to supply hole-type charge carriers into the CoO_2 layers [28]. Considering a constant oxygen composition and based on the valence equilibrium, the substitution of Ag^{+} for Ca^{2+} will create more electrical holes, and thus decrease ρ. Since the substitution happens at the [Ca_2CoO_3] layers, which do not disturb the CoO_2 sub-lattice, the polaron hopping energy remains constant and the transport mechanism is therefore unchanged by the Ag-doping. On the other hand, for the heavily Ag-doped samples Ag03 and Ag04, the metallic-like electrical transport behavior arises from the existence of the secondary metallic Ag phase as confirmed by XRD and XPS analysis. In the dense and highly oriented $Ca_3Co_4O_9$ thin films, Ag clusters are likely to locate at grain boundaries, stacking faults and interfaces, and form connections between cobaltite grains. At low temperature, carrier scattering effect at the structural defects is not pronounced, and hence the electrical resistivity of Ag03 and Ag04 can be reduced effectively by metallic Ag. However, at high temperature above 600 K, the polaron hopping process of $Ca_3Co_4O_9$ will be greatly influenced by the presence of metallic Ag. In addition, much more structure defects and grain boundaries can act as scattering centers and eliminate the low energy carriers. It can be imagined that such scattering effect is more severe at high temperature. As a result, the Ag03 and Ag04 samples exhibit higher ρ at the high temperature range. For the individual composition, $\rho_{Ag} < \rho_{Ca_3Co_4O_9}$. So carriers would transport through Ag clusters rather than $Ca_3Co_4O_9$ grains in the composite structure, and electrical transportation of Ag03 and Ag04 changes into metallic-like behavior. [21].

Temperature dependence of the in-plane Seebeck coefficient, *S*, for pure and Ag-doped $Ca_3Co_4O_9$ thin films is plotted in Fig. 6. The positive sign of *S* for all the thin film samples indicates that hole carrier is still dominant in these samples, which is consistent with the Hall effect results. In addition, *S* values of the Ag-doped $Ca_3Co_4O_9$ thin films show similar trends

as the pure $Ca_3Co_4O_9$ thin film, namely, *S* increases with increasing temperature over the entire temperature range measured. It is also clearly shown that *S* decreases slightly with increasing Ag content for thin films Ag01 and Ag02, while decreases significantly for thin films Ag03 and Ag04. Ag04 exhibits the lowest *S* in the temperature range studied. This dependence of *S* on the Ag-doping amounts is also found to be consistent with that reported for Ag-doped $Ca_3Co_4O_9$ poly-crystalline bulk materials [29]. In the $Ca_3Co_4O_9$ system, *S* can be expressed by the Mott formula as [14]:

$$S(T) = \frac{c_e}{p} + \frac{\pi^2 k_B^2 T}{3e}\left[\frac{\partial \ln \mu(\varepsilon)}{\partial \varepsilon}\right]_{\varepsilon=E_F} \quad \text{(Eq. 2)}$$

where c_e is the electronic specific heat. It has been reported that for $Ca_3Co_4O_9$-based materials, *S* follows with the Drude picture: $S \sim c_e/p$, where the first term in Eq. 2 is dominant [14]. Therefore, for thin films Ag01 and Ag02, the increase in carrier concentration, *p*, can directly result in the decrease in Seebeck coefficient. However, for samples Ag03 and Ag04 multiphase system, the modification of effective carrier concentration becomes insignificant. Instead, the decrease in *S* in these two samples should be attributed to the existence of the metallic Ag phase within the $Ca_3Co_4O_9$ thin films. For materials with more than one type of charge carriers, the Seebeck coefficient could be expressed as [22]

$$S = \sum_i \left(\frac{\sigma_i}{\sigma}\right) S_i \,, \quad \text{(Eq. 3)}$$

and for samples Ag03 and Ag04 it can be rewritten as

$$S = \frac{\sigma_{Ca_3Co_4O_9}}{\sigma_{Ca_3Co_4O_9} + \sigma_{Ag}} S_{Ca_3Co_4O_9} + \frac{\sigma_{Ag}}{\sigma_{Ca_3Co_4O_9} + \sigma_{Ag}} S_{Ag} \,, \quad \text{(Eq. 4)}$$

which can be transformed into

$$S = S_{Ca_3Co_4O_9} + \frac{\sigma_{Ag}}{\sigma_{Ca_3Co_4O_9} + \sigma_{Ag}} \left(S_{Ag} - S_{Ca_3Co_4O_9}\right) \quad , \quad \text{(Eq. 5)}$$

since S_{Ag} is much smaller than $S_{Ca3Co4O9}$, and the second term in Eq. 5 is negative. As a result, *S* of $Ca_3Co_4O_9$/Ag multi-phase material can be expected to be lower than that of the single phase $Ca_3Co_4O_9$ system. And the decrease in *S* for thin films Ag03 and Ag04 can be observed.

Finally, the temperature dependence of power factor, *P*, of the pure and Ag-doped $Ca_3Co_4O_9$ thin films, was calculated from the measured ρ and *S* and plotted as shown in Fig. 7. For all samples, *P* values increase with increasing temperature. In addition, thin films Ag01 and Ag02 show higher power factor due to the positive enhancement on carrier concentration and mobility through the successful Ag-substitution at Ca site. Despite the increase in Ag amount, samples Ag03 and Ag04 exhibit decreasing *P* values because *S* is much suppressed by the presence of the metallic Ag phase. Among these thin film samples, the highest *P* value reaches ~0.73 mW/(mK^2) for thin film Ag02 at 705 K, which is about 16% higher than that of the pure $Ca_3Co_4O_9$ thin film and is among the best values reported for $Ca_3Co_4O_9$ materials [3, 22]. The present results have demonstrated the great potential of Ag-doped $Ca_3Co_4O_9$ thin films for thermoelectric applications. Meanwhile, the understanding of the influences of both Ag-substitution and Ag-addition has also shed light on the future effort of carrier tuning by cation-doping towards the improvement of TE performance.

4. Conclusions

In summary, Ag-doped $Ca_3Co_4O_9$ thin films with *c*-axis orientation have been prepared by PLD method. Careful characterization of the Ag-$Ca_3Co_4O_9$ thin films revealed that substitution limit of Ag at Ca site is only about 5 at% in $Ca_3Co_4O_9$ thin films. For the thin films doped with higher amount of Ag, excess Ag is found to exist as isolated metallic phase in the films. In addition, Ag^+ and Ag^0 doping in $Ca_3Co_4O_9$ thin films give different influences on the in-plane electrical properties. Ag^+-substitution at the Ca site can increase both the carrier concentration and mobility. As a result, despite a slight reduction in Seebeck coefficient, the in-plane electrical resistivity can be drastically decreased, contributing to the great enhancement in the power factor. However, for the heavily doped samples with Ag^0 phase, although the resistivity can be further decreased, Seebeck coefficient is severely reduced simultaneously. Among these Ag-doped $Ca_3Co_4O_9$ thin films, the highest power factor of ~0.73 mWm^{-1}K^{-2} was achieved for thin film Ag02 ($Ca_{2.88}Ag_{0.15}Co_4O_9$) at 705 K, which is about 16% higher than that of the pure $Ca_3Co_4O_9$ thin film. This indicates the great potential of Ag-doped $Ca_3Co_4O_9$ thin films for thermoelectric applications.

References

[1] J.G. Noudem, S. Lemonnier, M. Prevel, E.S. Reddy, E. Guilmeau, C. Goupil, J. Eur. Ceram. Soc. 28 (2008) 41-48.

[2] F.J. DiSalvo, Science 285 (1999) 703-706.

[3] M. Shikano, R. Funahashi, Appl. Phys. Lett. 82 (2003) 1851-1853.

[4] A.C. Masset, C. Michel, A. Maignan, M. Hervieu, O. Toulemonde, F. Studer, B. Raveau, J. Hejtmanek, Phys. Rev. B 62 (2000) 166-175.

[5] S. Horii, I. Matsubara, M. Sano, K. Fujie, M. Suzuki, R. Funahashi, M. Shikano, W. Shin, N. Murayama, J. Shimoyama, K. Kishio, Jpn. J. Appl. Phys. 42 (2003) 7018-7022.

[6] L.D. Hicks, M.S. Dresselhaus, Phys. Rev. B 47 (1993) 12727-12731.

[7] Y. Deng, H.M. Liang, Y. Wang, Z.W. Zhang, M. Tan, J.L. Cui, J. Alloys Compd. 509 (2011) 5683-5687.

[8] A. Sakai, T. Kanno, S. Yotsuhashi, A. Odagawa, H. Adachi, Jpn. J. Appl. Phys. 44 (2005) L966-L969.

[9] T. Sun, J. Ma, Q.Y. Yan, Y.Z. Huang, J.L. Wang, H.H. Hng, J. Cryst. Growth 311 (2009) 4123-4128.

[10] R. Moubah, S. Colis, C. Ulhaq-Bouillet, A. Dinia, Appl. Phys. Lett. 96 (2010) 041902.

[11] J. Lybeck, M. Valkeapaa, S. Shibasaki, I. Terasaki, H. Yamauchi, M. Karppinen, Chem. Mater. 22 (2010) 5900-5904.

[12] K. Sugiura, H. Ohta, K. Nomura, M. Hirano, H. Hosono, K. Koumoto, Appl. Phys. Lett. 89 (2006) 032111.

[13] M.G. Kang, K.H. Cho, S.M. Oh, J.S. Kim, C.Y. Kang, S. Nahm, S.J. Yoon, Appl. Phys. Lett. 98 (2011) 142102.

[14] G.J. Xu, R. Funahashi, M. Shikano, I. Matsubara, Y.Q. Zhou, Appl. Phys. Lett. 80 (2002) 3760-3762.

[15] F. Delorme, C.F. Martin, P. Marudhachalam, D.O. Ovono, G. Guzman, J. Alloys Compd. 509 (2011) 2311-2315.

[16] N.V. Nong, C.J. Liu, M. Ohtaki, J. Alloys Compd. 509 (2011) 977-981.

[17] J. Pei, G. Chen, N. Zhou, D.Q. Lu, F. Xiao, Physica B: Condensed Matter 406 (2011) 571-574.

[18] Q. Yao, D.L. Wang, L.D. Chen, X. Shi, M. Zhou, J. Appl. Phys. 97 (2005) 103905.

[19] Y. Wang, Y. Sui, J. Cheng, X.J. Wang, J.P. Miao, Z.G. Liu, Z.N. Qian, W.H. Su, J. Alloys Compd. 448 (2008) 1-5.

[20] P.H. Xiang, Y. Kinernuchi, H. Kaga, K. Watari, J. Alloys Compd. 454 (2008) 364-369.

[21] M. Mikami, N. Ando, R. Funahashi, J. Solid State Chem. 178 (2005) 2186-2190.

[22] Y. Wang, Y. Sui, J.G. Cheng, X.J. Wang, W.H. Su, J. Alloys Compd. 477 (2009) 817-821.

[23] T. Sun, H.H. Hng, Q.Y. Yan, J. Ma, J. Appl. Phys. 108 (2010) 083709.

[24] M. Lorenz, H. Hochmuth, D. Natusch, M. Kusunoki, V.L. Svetchnikov, V. Riede, I. Stanca, G. Kastner, D. Hesse, IEEE Transactions on Applied Superconductivity 11 (2001) 3209-3212.

[25] L.S.J. Peng, X.X. Xi, B.H. Moeckly, S.P. Alpay, Appl. Phys. Lett. 83 (2003) 4592-4594.

[26] D.I. Garcia-Gutierrez, M. José-Yacamán, S. Lu, D.Q. Kelly, S.K. Banerjee, J. Appl. Phys. 100 (2006) 044323.

[27] Y. Chen, X.L. Xu, G.H. Zhang, H. Xue, S.Y. Ma, Physica B-Condensed Matter 404 (2009) 3645-3649.

[28] Y. Miyazaki, M. Onoda, T. Oku, M. Kikuchi, Y. Ishii, Y. Ono, Y. Morii, T. Kajitani, J. Phys. Soc. Jpn. 71 (2002) 491-497.

[29] F.P. Zhang, Q.M. Lu, J.X. Zhang, X. Zhang, J. Alloys Compd. 477 (2009) 543-546.

Table and Figure captions

Tab. 1. Chemical compositions of sol-gel solutions, PLD targets and the as-prepared thin films as well as their thicknesses.

Sample Name	Sol-gel solution Ca: Ag: Co	Target Ca: Ag: Co	Thin Film Composition			Film thickness (nm)
			Ca: Ag: Co	Ag^{+}: Ag^{0} (%)	Nominal Formula	
CCO	3: 0: 4	3.04 : 0.00 : 4	3.02: 0.00: 4	–	$Ca_3Co_4O_9$	99.(8)
Ag01	2.9: 0.2: 4	2.91 : 0.21 : 4	2.93: 0.07: 4	100: 0	$Ca_{2.93}Ag_{0.072}Co_4O_9$	107.(7)
Ag02	2.8: 0.4: 4	2.81 : 0.40 : 4	2.89: 0.15: 4	100: 0	$Ca_{2.89}Ag_{0.151}Co_4O_9$	102.(3)
Ag03	2.7: 0.6: 4	2.73 : 0.59 : 4	2.88: 0.22: 4	70.7: 29.3	$Ca_{2.88}Ag_{0.155}Co_4O_9/Ag_{0.064}$	108.(6)
Ag04	2.6: 0.8: 4	2.62 : 0.77 : 4	2.86: 0.29: 4	53.9: 46.1	$Ca_{2.86}Ag_{0.156}Co_4O_9/Ag_{0.134}$	98.(8)

Fig. 1. HR-XRD long-scan patterns of pure and Ag-doped $Ca_3Co_4O_9$ thin films.

Fig. 2. Relationship between *c*-axis parameter (calculated from the 2θ angle of (00*l*) peaks) and Ag content (determined by XPS by assessing Co = 4).

Fig. 3. (Color online) XPS fine scan spectra of Ag 3d (5/2) and (3/2) for Ag-doped $Ca_3Co_4O_9$ thin films.

Fig. 4. (Color online) Temperature dependence of in-plane electrical resistivity, ρ, for pure and Ag-doped $Ca_3Co_4O_9$ thin films. The inset gives Ag content dependence of carrier concentration, *p*, and carrier mobility, μ.

Fig. 5. (Color online) Plot of $\ln(\rho/T)$ versus $1000/T$ for pure and Ag-doped $Ca_3Co_4O_9$ thin films. The lines denote the linear fitting. And the inset gives the evaluated activation energy, E_a.

Fig. 6. (Color online) Temperature dependence of in-plane Seebeck coefficient, *S*, for pure and Ag-doped $Ca_3Co_4O_9$ thin films.

Fig. 7. (Color online) Temperature dependence of in-plane power factor, *P*, for pure and Ag-doped $Ca_3Co_4O_9$ thin films.

Highlights

- Ag-doped *c*-axis oriented $Ca_3Co_4O_9$ thin films have been prepared by pulsed laser deposition.
- Ag substitution limit at Ca site is found to be ~5 at% and heavy Ag-doping results in composite structure.
- Ag-substitution increases carrier concentration and mobility; while Ag-compositing greatly reduces Seebeck coefficient.
- Power factor reaches ~0.73 $mWm^{-1}K^{-2}$, which is about 16% improvement.

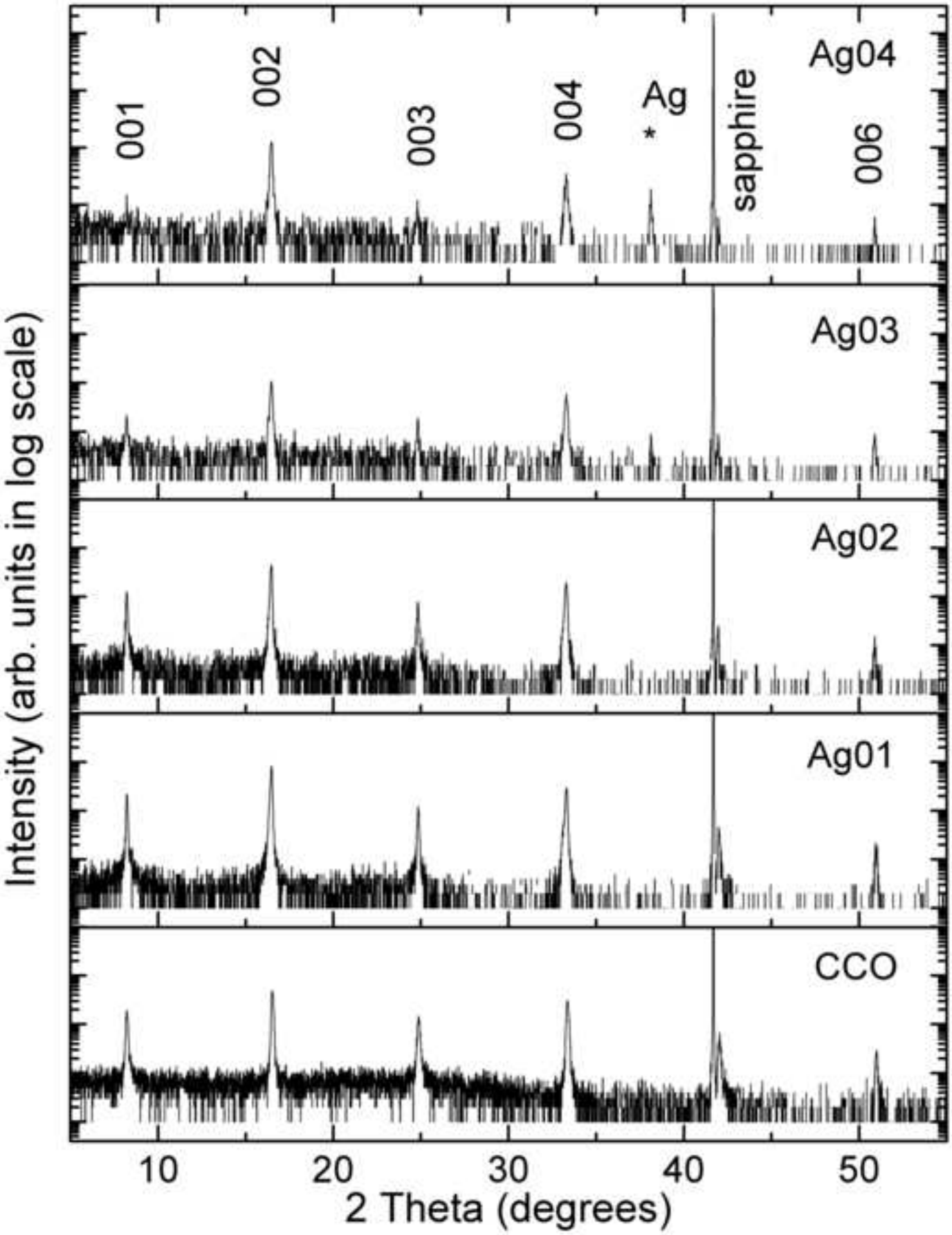

Figure2

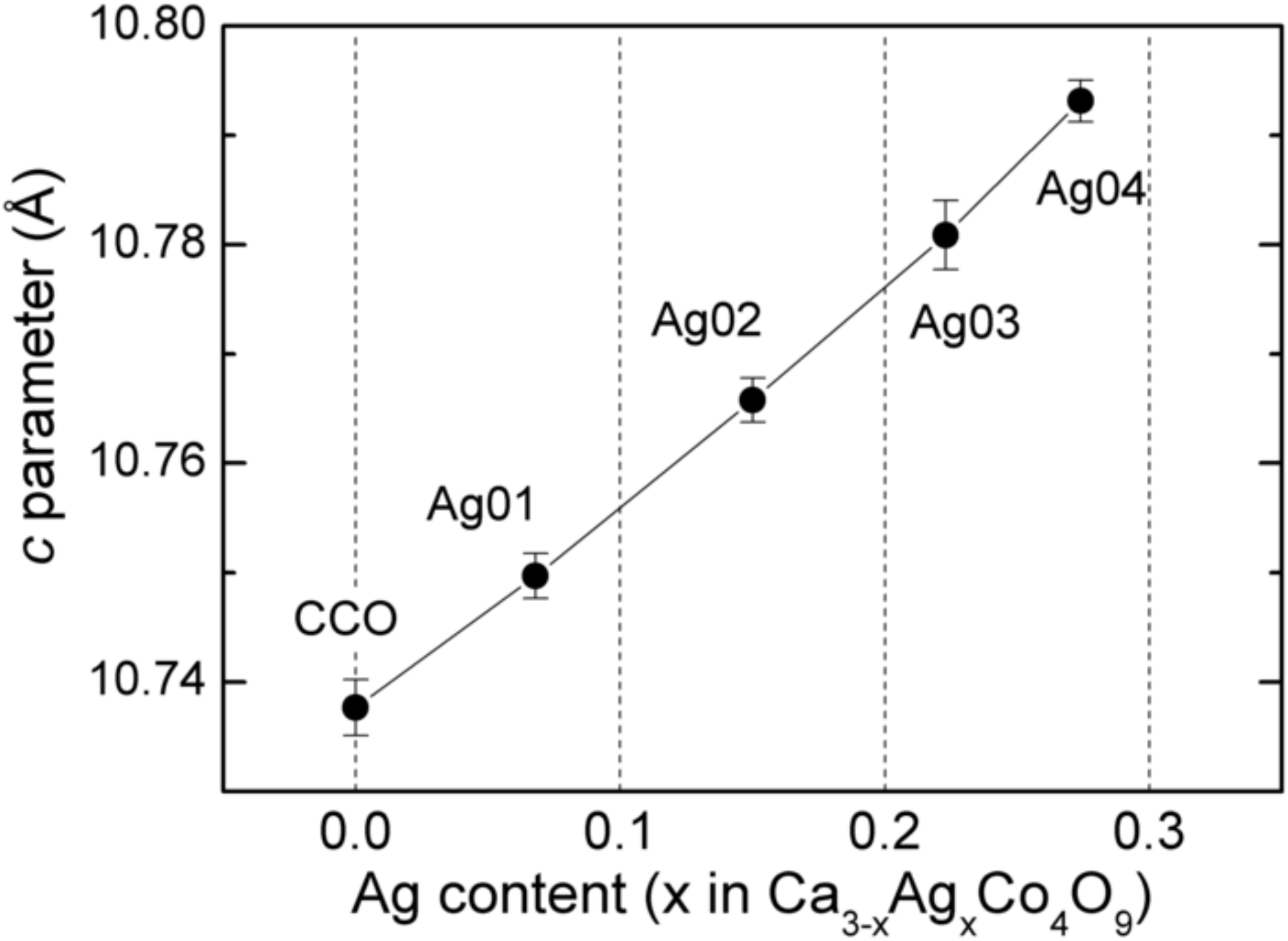
10.80
10.78
10.76
10.74
c parameter (Å)
CCO
Ag01
Ag02
Ag03
Ag04
0.0
0.1
0.2
0.3
Ag content (x in Ca3-xAgxCo4O9)

Figure3

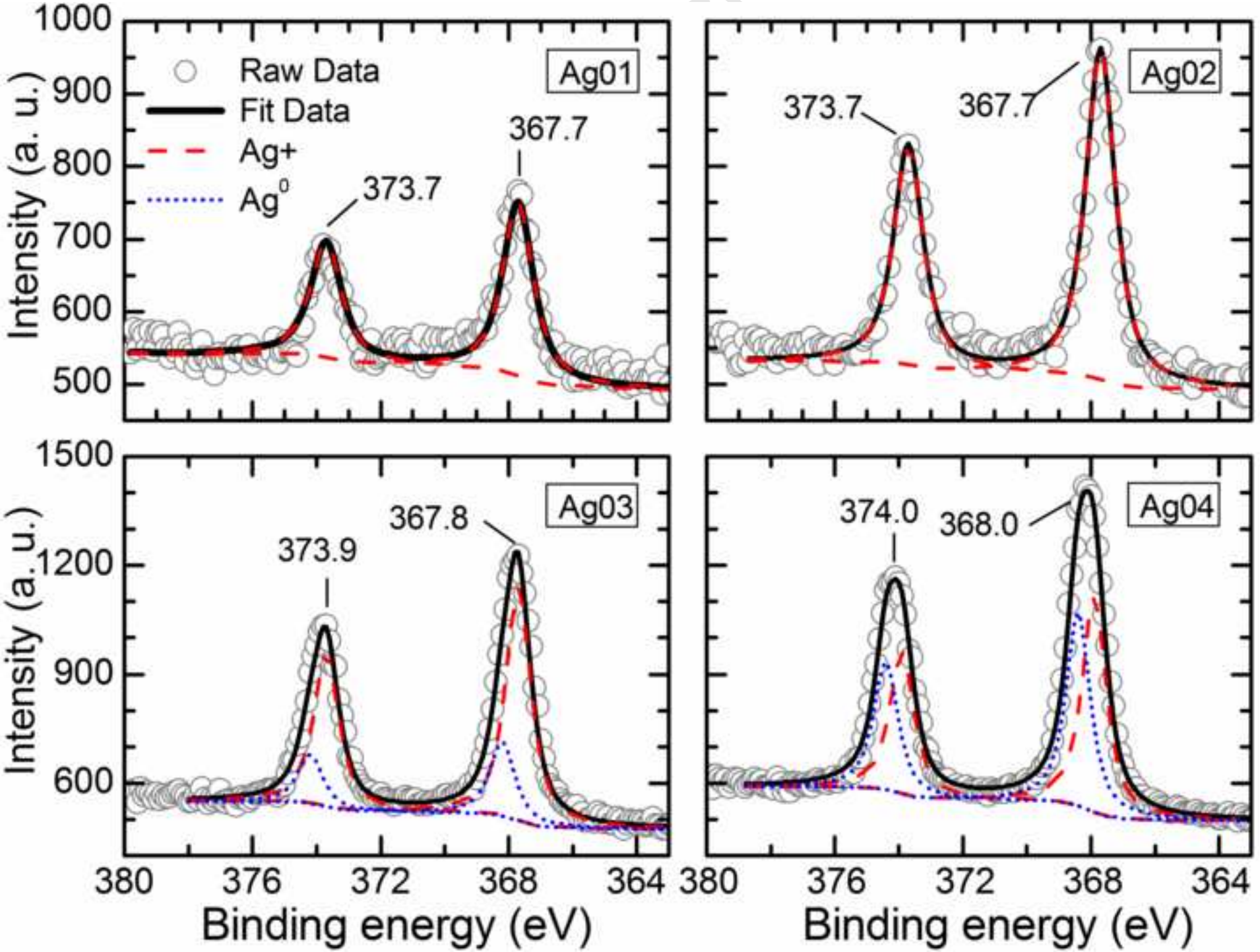
Raw Data
Fit Data
Ag+
Ag0
Ag01
373.7
367.7
Ag02
373.7
367.7
Ag03
373.9
367.8
Ag04
374.0
368.0
Intensity (a. u.)
Binding energy (eV)
1000
900
800
700
600
500
1500
1200
900
600
380
376
372
368
364

Figure4

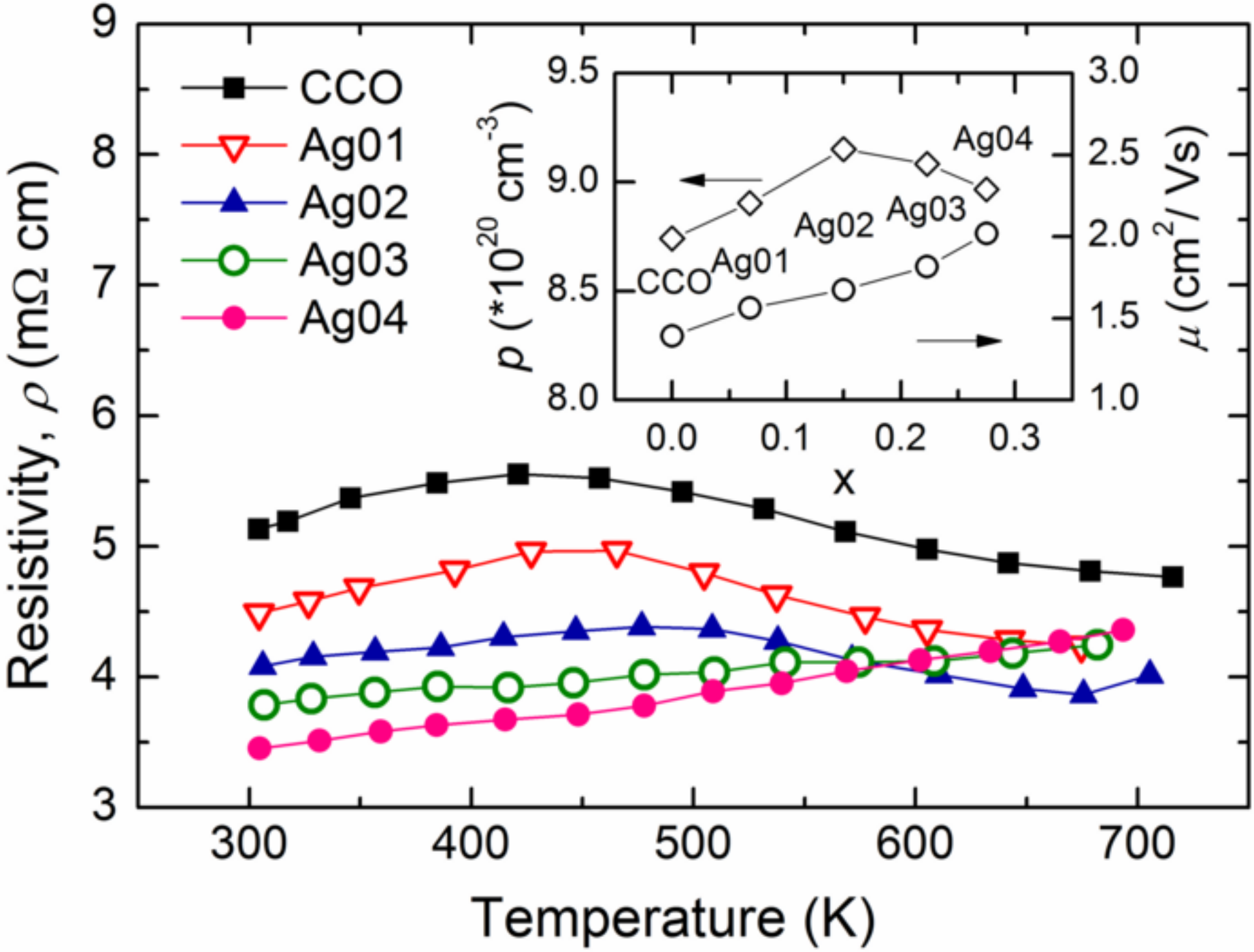
CCO
Ag01
Ag02
Ag03
Ag04
Resistivity, ρ (mΩ cm)
Temperature (K)
300
400
500
600
700
3
4
5
6
7
8
9
p (*10^20 cm^-3)
μ (cm^2/ Vs)
x
0.0
0.1
0.2
0.3
8.0
8.5
9.0
9.5
1.0
1.5
2.0
2.5
3.0

Figure5

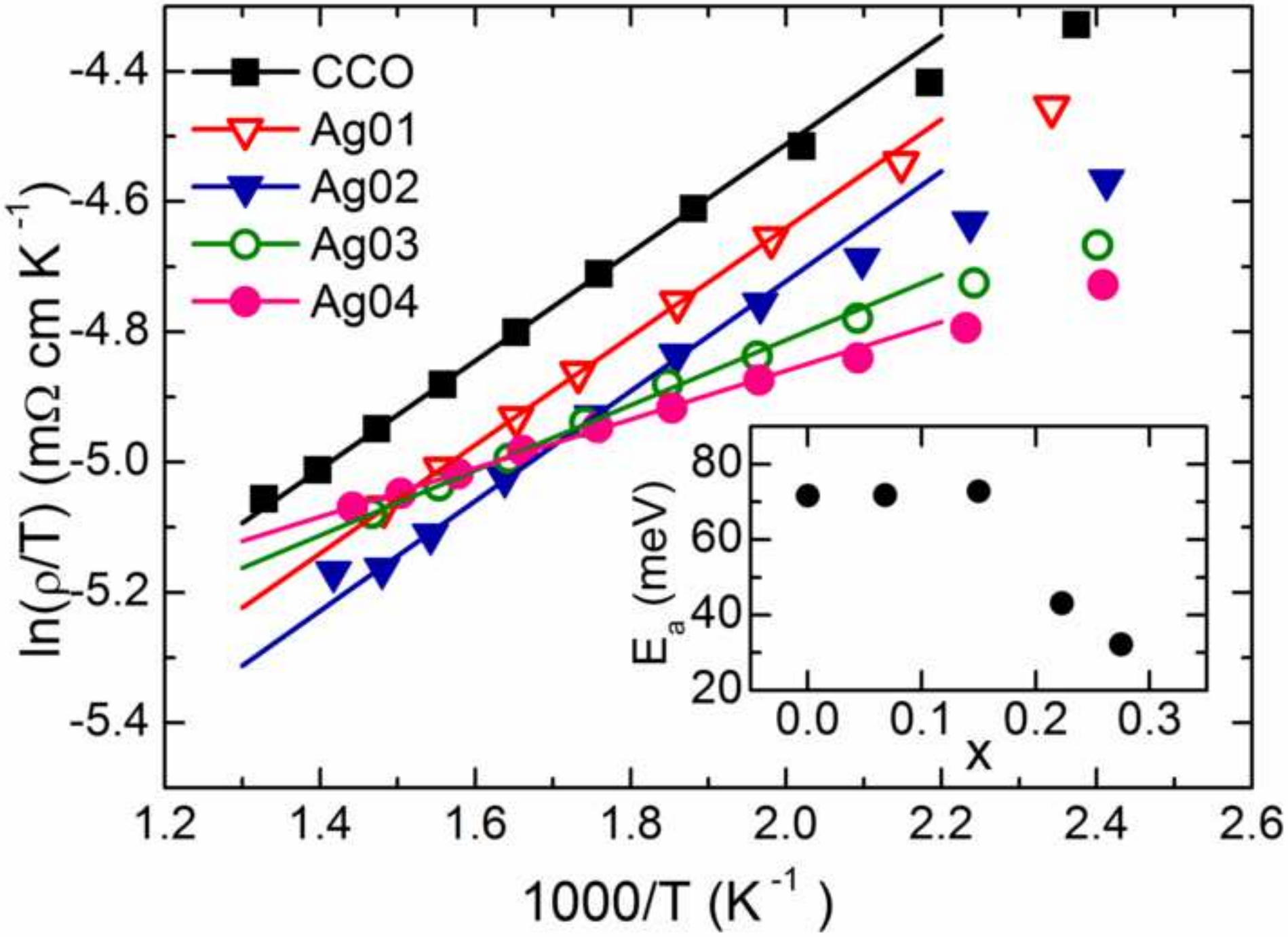
CCO
Ag01
Ag02
Ag03
Ag04
ln(ρ/T) (mΩ cm K-1)
-4.4
-4.6
-4.8
-5.0
-5.2
-5.4
1.2
1.4
1.6
1.8
2.0
2.2
2.4
2.6
1000/T (K-1)
Ea (meV)
80
60
40
20
0.0
0.1
0.2
0.3
x

Figure6

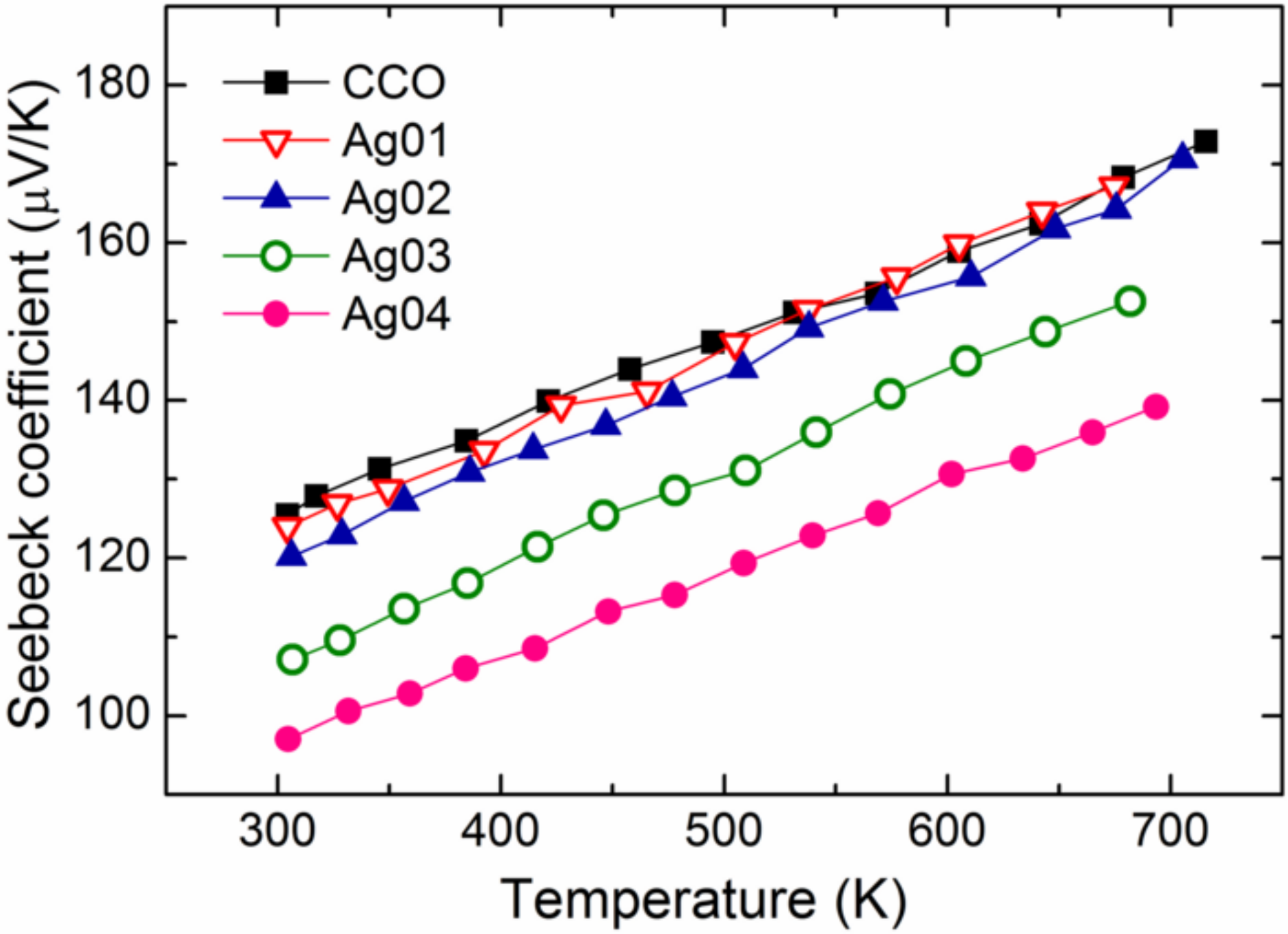
CCO
Ag01
Ag02
Ag03
Ag04
Seebeck coefficient (μV/K)
180
160
140
120
100
300
400
500
600
700
Temperature (K)

Figure7

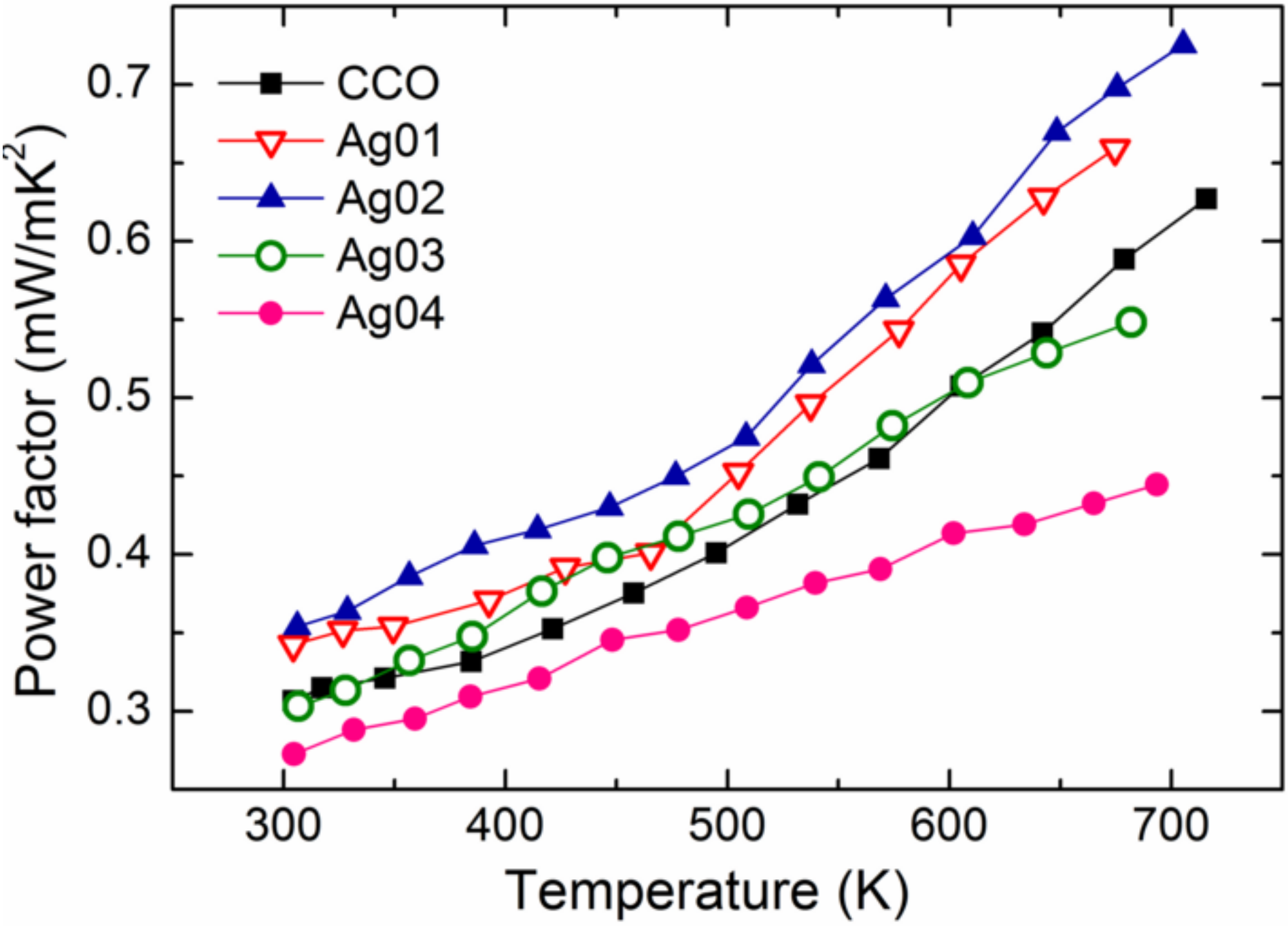
CCO
Ag01
Ag02
Ag03
Ag04
Power factor (mW/mK^2)
0.3
0.4
0.5
0.6
0.7
300
400
500
600
700
Temperature (K)